

Cite this: *Soft Matter*, 2012, **8**, 11839

www.rsc.org/softmatter

PAPER

Partitioning of ethanol into lipid membranes and its effect on fluidity and permeability as seen by X-ray and neutron scattering

Laura Toppozini,^{*a} Clare L. Armstrong,^a Matthew A. Barrett,^a Songbo Zheng,^a Lindy Luo,^a Hirsh Nanda,^b Victoria García Sakai^{*c} and Maikel C. Rheinstädter^{*ad}

Received 3rd July 2012, Accepted 11th September 2012

DOI: 10.1039/c2sm26546j

We present a combined neutron and X-ray scattering investigation to study the effect of ethanol on the molecular structure and dynamics of lipid membranes. 1,2-Dimyristoyl-*sn*-glycero-3-phosphatidylcholine (DMPC) powder hydrated with a 5 wt% ethanol solution (corresponding to 2 mol% of ethanol) was used in this study. From high-resolution X-ray experiments the position and partitioning of the ethanol molecules in the phospholipid bilayers was determined in their gel and fluid phases. We find that the ethanol molecules reside in the head group region of the bilayers, with 1.6 ethanol molecules per lipid molecule in the gel phase and 1.2 ethanol molecules per lipid molecule in the fluid phase. We find evidence for enhanced permeability in both fluid and gel phases of the phospholipid bilayers in the presence of ethanol molecules. Elastic and quasi-elastic neutron scattering data, obtained using a neutron backscattering spectrometer, was used to study slow, nanosecond molecular dynamics on length scales corresponding to lipid diffusion, acyl chain dynamics and solvent dynamics. While the presence of ethanol molecules had no observable effect on these types of dynamics in the fluid (L_α) phase, the membranes appeared to have a higher degree of order in gel (L_β) and ripple (P_β) phases. In particular, lipid diffusion was found to be slower by a factor of two in the more rigid gel phase when ethanol was present.

1 Introduction

Our knowledge about interactions between ethanol and lipid membranes on the molecular scale mainly stems from two techniques: nuclear magnetic resonance (NMR) experiments^{1–3} and molecular dynamics (MD) simulations.^{4–9} In particular, experiments using neutron and X-ray scattering to probe molecular dynamics and structure are scarce,^{10–12} most likely due to experimental challenges.

When partitioning into the bilayer, ethanol has been found to reside predominately at the membrane–water interface. Ethanol's hydrophilic nature causes it to exhibit a lower degree of partitioning into the hydrophobic core of the bilayer, differing from longer chain alcohols that insert into the hydrophobic core with their hydrophobic chains aligned parallel to the lipid hydrocarbon chains.^{7,13} The ethanol molecules can form hydrogen bonds with the lipid head groups with bond lifetimes of about 1 nanosecond.^{7,14} It has been reported that ethanol has

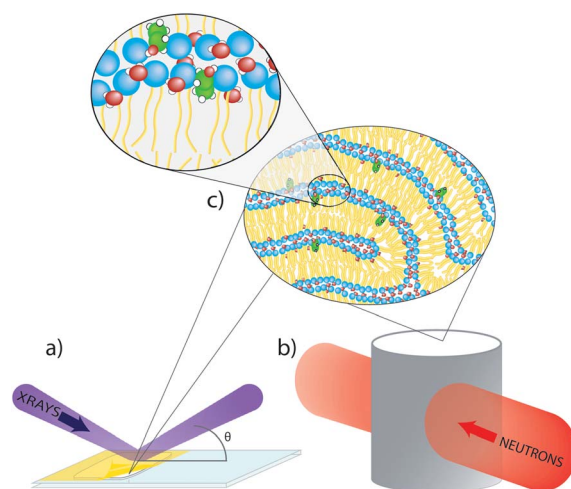


Fig. 1 Schematic diagram of the X-ray and neutron scattering experiments performed on a hydrated lipid powder. (a) The powder was applied to a ~ 0.5 mm depression in a glass slide for X-ray experiments. A $13 \mu\text{m}$ thick Kapton sheet was placed over the depression to avoid evaporation. (b) In the neutron scattering experiment, hydrated powder was applied to the sides of a annular aluminium sample holder. (c) Cartoon of the membrane structure in the hydrated powder, notice the non-oriented bilayer formation. DMPC: blue; H_2O : red; ethanol: green.

^aDepartment of Physics and Astronomy, McMaster University, Hamilton, ON, Canada. E-mail: toppozl@mcmaster.ca; rheinstadter@mcmaster.ca

^bNIST Center for Neutron Research, National Institute of Standards and Technology, Gaithersburg, MD, USA

^cISIS Pulsed Neutron and Muon Source, Rutherford Appleton Laboratory, Didcot, UK. E-mail: victoria.garcia-sakai@stfc.ac.uk

^dCanadian Neutron Beam Centre, National Research Council Canada, Chalk River, ON, Canada

numerous effects on the lipid bilayer: it decreases the gel-to-fluid transition temperature,^{1,4} it has a weak effect on the area per lipid, and it increases membrane fluidity and disorder.⁷ Finally, and perhaps most importantly, ethanol has been found to increase membrane permeability.^{7,15,16}

The aim of this study is to determine molecular structure and dynamics of phospholipid membranes hydrated by a 5 wt% ethanol solution. This concentration is significantly larger than the typical, very low alcohol concentrations of ~ 0.092 wt% (~ 0.036 mol%) found in human blood.² However, 5 wt% can be considered a moderate alcohol concentration to which skin and mucous membranes in the mouth and digestive system can be exposed. We combined elastic and quasi-elastic neutron scattering and X-ray diffraction to study the properties of multi-lamellar lipid bilayers containing ethanol. Using neutron scattering, we determined the impact of ethanol on slow, nanosecond membrane dynamics at different length scales, such as lipid diffusion, nanoscale tail dynamics and hydration water dynamics. While ethanol did not alter dynamics in the fluid phase, the ripple and gel phases exhibited a higher degree of molecular order with slower dynamics. The lipid diffusion constant showed a significant 50% decrease in the gel phase of the membranes. From the X-ray scattering experiments, we were able to determine the position of the ethanol molecules in the membrane and determine their partitioning, *i.e.*, the number of ethanol molecules per lipid molecule, in the bilayer. In addition, we found experimental evidence to suggest an increase in the permeability of the membranes due to the presence of ethanol.

2 Materials and methods

2.1 Sample preparation

To ensure a well defined ethanol concentration in the membranes, it is necessary that the bilayers are in direct contact with a water-ethanol solution. For this reason, hydrated lipid powders were used in this study. Highly concentrated suspensions of 1,2-dimyristoyl-*sn*-glycero-3-phosphatidylcholine (DMPC) were prepared by hydrating the lipid powder. Four types of samples were prepared, two for each scattering technique. In the dynamical neutron scattering experiments, lipids were hydrated with D₂O and D₂O-d-ethanol (deuterated ethanol) 5 wt%. In the X-ray scattering experiments, lipids were hydrated with ultra pure H₂O and an H₂O-5 wt% ethanol solution. The typical sample mass was ~ 300 mg for the neutron and ~ 15 mg for the X-ray experiment. A 3 : 1 mass ratio of water or water-ethanol solution to lipid powder was mixed to ensure full hydration of the bilayers. We envision the structure of the hydrated powder as depicted in the cartoon in Fig. 1 as a randomly oriented multi-lamellar structure. The number of water and ethanol molecules that attach to and incorporate into the bilayers change the concentration of the solution. About 7–8 water molecules per lipid molecule are found in the head group region of the bilayers;^{2,17} we find about 1.6 ethanol molecules per lipid molecule (as will be shown below). Using these numbers the concentration of the water-ethanol solution changes from 2 mol% to ~ 1 mol% when it is in contact with the lipid powder. The concentration of ethanol molecules in the membranes is, therefore, not limited by the total number of ethanol molecules available in the solution.

An annular sample cell made of aluminium was used for the neutron experiments. The suspension was applied as a film to the inner wall of the hollow cylinder after which, an inner cylinder was inserted to form a seal. The sample was mounted inside of a cryostat. A temperature range between 280 K $< T <$ 335 K was used, which covers the temperatures of gel (L_{β}), ripple (P_{β}) and fluid (L_{α}) phases of the bilayers. Temperature was controlled to better than 0.1 K.

In the X-ray experiments, the lipid mixture was spread on a ~ 20 mm \times 20 mm \times 0.5 mm square well ground into a Quartz glass slide. The hydrated powder was sealed with a 13 μ m thick Kapton polyimide foil acting as an X-ray window using vacuum grease for adhesion. The sample was mounted in a temperature controlled humidity chamber during the X-ray experiments. Temperature was controlled using a circulating water bath controller with a temperature stability of better than 0.1 K. The structure of the lipid-ethanol system was studied at two temperatures: 293 K, allowing observation of the gel (ripple, P_{β}) phase of the membranes, and 303 K, to observe their fluid (L_{α}) phase. Fig. 1 shows schematics of the neutron and X-ray scattering sample and the experimental geometries.

2.2 Neutron scattering experiment

The neutron experiments were carried out at the High Flux Neutron Backscattering Spectrometer (HFBS)²¹ at the NIST Center for Neutron Research (NCNR), Gaithersburg, in its standard set-up with Si(111) monochromator and analyzer crystals corresponding to an incident and analyzed neutron energy of 2.08 meV ($\lambda = 6.27$ Å). Two types of experiments were conducted: so-called elastic (fixed energy window, FEW) scans and quasi-elastic neutron scattering (QENS).

Elastic incoherent neutron scattering is an established tool for the detection of molecular freezing and melting,^{18,19,22–25} where sample scattering is recorded as a function of temperature. At the energy resolution of ~ 0.9 μ eV, only molecular motions with characteristic times slower than ~ 1 ns are monitored. The experiment covered lateral length scales of 3.5–12 Å to study dynamics down to nearest-neighbour distances of both lipid acyl tails and hydration water molecules. Performing elastic scans as a function of temperature, reveals dynamical changes on different length scales. Freezing and melting of molecular degrees of freedom can easily be identified because they lead to jumps or kinks in the recorded intensity, as shown below.

The 16 HFBS detectors (D1–D16) cover a total Q range of 0.14 Å⁻¹ to 1.81 Å⁻¹. Table 1 lists the centre Q -values and the corresponding length scales. Each detector covers an angular range of approximately 8°. Different types of motion fall into the length scales covered by the HFBS spectrometer.

Slow nanosecond dynamics of lipid and water molecules were studied previously using backscattering spectrometers by analyzing elastic scattering at the positions of the lipid acyl chain and hydration water correlation peaks.^{18–20,25,26} Based on these results, different types of dynamics can be distinguished based on their length scale dependence:

- Incoherent scattering is dominant at intermediate Q values, between about 0.3 and 1.5 Å⁻¹, where no correlation peak occurs. This range of length scales between ~ 4 and 21 Å is often used in neutron scattering studies (see, *e.g.* ref. 22 and 24) to study diffusion and molecular mean square displacements of

Table 1 Neutron detector (D1–D16), corresponding centre Q -value, length scales and type of scattering and motion detected. The lipid acyl chain correlation peak is centred at $Q \sim 1.5 \text{ \AA}^{-1}$. The hydration water correlation peak was reported at $Q = 1.85 \text{ \AA}^{-1}$ (ref. 18–20)

Detector	Q (\AA^{-1})	Distance (\AA)	Dominant scattering	Associated motion
D1	0.25	25		
D2	0.36	17		
D3	0.47	13		
D4	0.56	11		
D5	0.62	10		
D6	0.75	8	Incoherent	Lipid diffusion
D7	0.87	7		
D8	0.99	6.3		
D9	1.11	5.7		
D10	1.22	5.2		
D11	1.32	4.8		
D12	1.42	4.4		
D13	1.51	4.2	Lipid tail correlation peak	Lipid tail dynamics
D14	1.60	3.9		
D15	1.68	3.7		
D16	1.75	3.6	Hydration water correlation peak	Hydration water dynamics

lipid molecules. We assigned the Q -range from 0.69 \AA^{-1} to 1.17 \AA^{-1} (detectors D6–D9), to incoherent dynamics due to diffusion of lipid molecules, covering length scales from 5.6–9.2 \AA . These values take into account the Q -range for each detector.

- Detector D13, covers the Q range of the lipid acyl chain correlation peak ($\sim 1.5 \text{ \AA}^{-1}$) and was assigned to lipid tail fluctuations.

- The nearest-neighbour distance of the hydration water molecules leads to a correlation peak centred at 1.85 \AA^{-1} , corresponding to a nearest-neighbour distance of 3.4 \AA between hydration water molecules, slightly larger than bulk water. Detector D16 was, therefore, assigned to dynamics of hydration water molecules. We note that D16 is centred at 1.75 \AA^{-1} , however it covers the hydration correlation peak partially.

The multi-lamellar Bragg reflections due to stacking of the membranes are veritable Bragg peaks related to an order on basically infinite time scales, in both gel and fluid phases. The in-plane correlations related to lipid tails and water molecules, which lead to in-plane correlation peaks at high Q values above $\sim 0.7 \text{ \AA}^{-1}$, however, are dynamic in nature. It has been shown using energy resolved neutron diffraction¹⁸ that these correlations exist on time scales only up to nanoseconds in the fluid phase of the membranes. The absence of “true” elastic scattering is the fingerprint of a fluid structure; it is well known that lipid membranes show properties of a 2D fluid in their fluid phases. The corresponding reflections are usually observed in neutron and X-ray diffraction experiments as relatively weak and broad peaks as compared to the out-of-plane Bragg peaks. The scattering, which occurs at the peak positions of lipid acyl chain and hydration water molecules in our experiment is, therefore, not static but can be used to characterize the time scale of the underlying molecular degrees of freedom, as suggested in ref. 18, 19, 25 and 26 and in Table 1.

Lipid diffusion, and lipid tail and hydration water dynamics were studied simultaneously by analyzing different detectors.

Table 1 lists the dominant scattering contribution for different length scales and corresponding motion observed in the various detectors. Because the HFBS detectors have a coarse angular (Q) resolution of approximately 8° each, the experiment was not sensitive to shifts of the lipid and water correlation peak with temperature due to potential structural changes of the bilayers with temperature. The measured elastic intensity at the Q position for diffusion, lipid tail and hydration water dynamics is shown in Fig. 2. The scans cover a temperature range of $280 \text{ K} < T < 335 \text{ K}$. Data were taken in heating and cooling scans at a rate

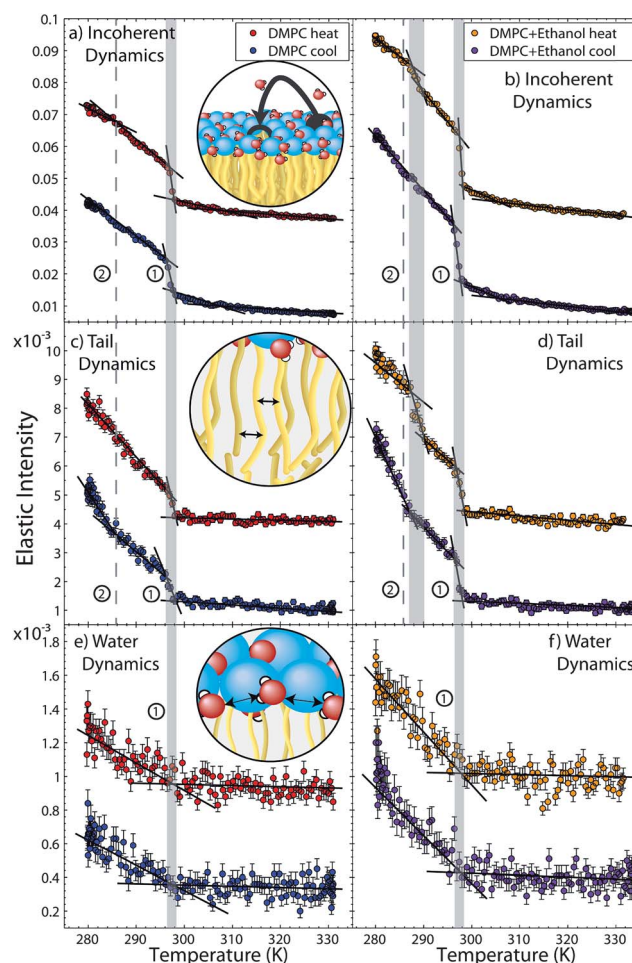


Fig. 2 The elastic neutron scattering experiment was sensitive to lipid diffusion, lipid acyl chain and hydration water dynamics. As listed in Table 1, data from detectors D6 through D9 were summed to create the lipid diffusion plots, detector D13 data for lipid acyl chain dynamics, and detector D16 data for hydration water dynamics. Heating and cooling scans are shown. All heating curves are shifted upward in intensity for clarity; the original data show closed loops. Error bars represent one standard deviation. The experimental temperature resolution was 0.5 K. The temperature of the pre-transition in pure DMPC is marked by a dashed line. The shaded areas marks the ranges of pre- and main transitions. The error in the determination of the transition temperatures is related to the determination of the intersection of the different slopes. For lipid dynamics we estimate the maximum error to be $\sim 2 \text{ K}$ as determined by min./max. slopes. The hydration water data in (c) has slightly larger statistical errors (*i.e.* lower detector counts due to its placement within the instrument) and the maximum error in the determination of the transition temperature was estimated to be $\sim 4 \text{ K}$.

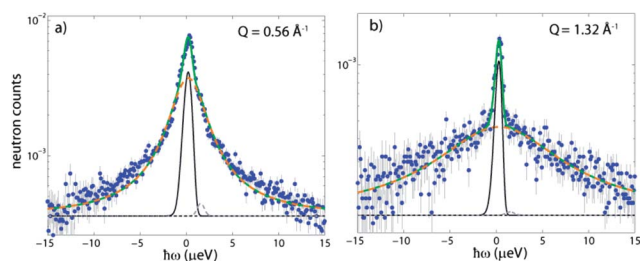


Fig. 3 QENS spectra of the DMPC–ethanol sample at $T = 308$ K recorded at low (a) and high (b) Q -values. The instrumental resolution is fit with two functions: an asymmetric Gaussian (solid black curve) and a second Gaussian function (dashed grey curves). The quasi-elastic broadening is fit with a Lorentzian (dashed orange curve) and a constant background (dashed black line), and the total fit is shown as a solid green curve.

of 0.5 K min^{-1} . Because the counting time was set to 1 min, the temperature resolution of the experiment is determined to be 0.5 K.

Quasi-elastic neutron scattering is a powerful tool to gain access to slow nanosecond molecular dynamics in soft-matter and biophysics, see *e.g.* ref. 27 for a recent review. Neutron spectra are recorded in quasi-elastic neutron scattering experiments. A mechanical Doppler drive was employed to produce an oscillatory motion of the monochromator in order to vary the incident energy of the neutrons. A dynamic range of $-15 \mu\text{eV} < \hbar\omega < 15 \mu\text{eV}$ is accessible using this set-up. The corresponding spectra are shown in Fig. 3. By analyzing the shape of the inelastic scattering, detailed information about nanosecond molecular dynamics in the membranes can be obtained. We used quasi-elastic scattering to determine lipid diffusion coefficients at selected temperatures, as will be shown below. Phase transitions were determined first using the elastic scans. Diffusion was then measured in the gel and fluid phases using QENS.

2.3 X-ray scattering experiment

X-ray scattering data were obtained using the Biological Large Angle Diffraction Experiment (BLADE) in the Laboratory for Membrane and Protein Dynamics at McMaster University. BLADE uses a 9 kW (45 kV, 200 mA) CuK α rotating anode at a wavelength of 1.5418 Å. Both source and detector are mounted on movable arms ensuring the sample stay horizontal during the measurements. Multi-layer focussing optics provide a high intensity beam with monochromatic X-ray intensities up to 10^{10} photons/(mm $^2 \times \text{s}$). Data were obtained in reflection geometry using a collimated X-ray beam. A schematic of the scattering geometry is shown in Fig. 1(a).

The scans, as shown in Fig. 4, cover a Q range up to 2.5 \AA^{-1} , which extends over length scales from intermolecular distances to the lamellar spacing between neighbouring membranes. As the multi-lamellar membranes are not oriented, Bragg peaks due to the lamellar stacking perpendicular to the membranes and in-plane correlation peaks due to molecular alignment in the plane of the membranes, are observed simultaneously. The lamellar Bragg peaks are observed in the Q range between ~ 0.1 and $\sim 0.75 \text{ \AA}^{-1}$, corresponding to lamellar spacings of $\sim 65 \text{ \AA}$. The lipid acyl chain correlation peak in DMPC occurs at a Q value

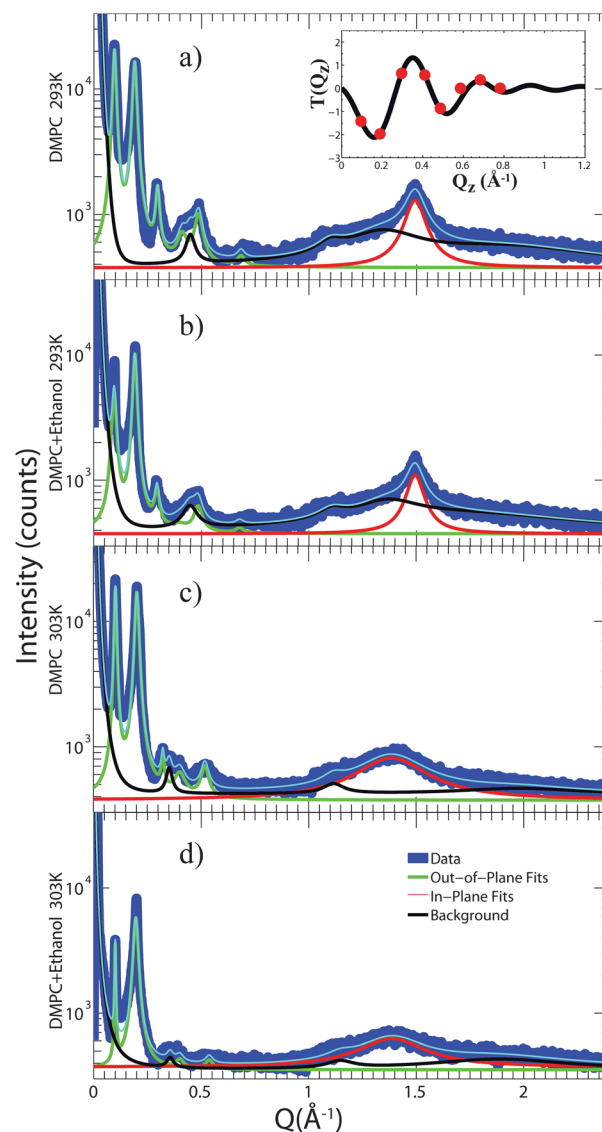


Fig. 4 Overview of the X-ray data. (a) DMPC at $T = 293$ K (gel phase). The inset shows $T(Q_z)$, as defined in eqn (2). (b) DMPC–ethanol at $T = 293$ K (gel phase), (c) DMPC at $T = 303$ K (fluid phase), (d) DMPC–ethanol at $T = 303$ K (fluid phase). Background of the sample holder was subtracted from the data in (a)–(d). The total fit is shown in light blue. The low- Q scans were assigned to a multi-lamellar membrane structure and shown in green. The inter-acyl chain correlation peak at Q values of $\sim 1.5 \text{ \AA}^{-1}$ is shown in red. The weak intensity at $\sim 1.1 \text{ \AA}^{-1}$ stems from the Kapton window and did not subtract perfectly.

of $\sim 1.5 \text{ \AA}^{-1}$ in the gel phase,^{18,28} below the main phase transition at $T = 296.6$ K.

The multi-lamellar Bragg peaks allow for the determination of the structure perpendicular to the plane of the membranes (see, *e.g.* ref. 29 and 30 for recent reviews). Because of the membrane stacking, *i.e.* the convolution with the lamellar structure factor, the Fourier transform is not continuous but discrete. The different Fourier components are observed in the experiment as the integrated intensities of the out-of-plane Bragg peaks. The electron density, $\rho(z)$, can be approximated by a 1D Fourier analysis:³¹

$$\begin{aligned}\rho(z) &= \rho_w + \frac{F(0)}{d_z} + \frac{2}{d_z} \sum_{n=1}^N F(q_n) v_n \cos(q_n z) \\ &= \rho_w + \frac{F(0)}{d_z} + \frac{2}{d_z} \sum_{n=1}^N \sqrt{I_n} q_n v_n \cos\left(\frac{2\pi n z}{d_z}\right)\end{aligned}\quad (1)$$

N is the highest order of the Bragg peaks observed in the experiment and ρ_w the electron density of water or solution. The integrated peak intensities, I_n , are multiplied by q_n and square rooted to obtain the form factors, $F(q_n)$.^{32,33} The bilayer form factor $F(q_z)$, which is in general a complex quantity, is real-valued in the case of centro-symmetry. The phase problem of crystallography, therefore, simplifies to the sign problem $F(q_z) = \pm|F(q_z)|$. The phases, v_n , can only take the values ± 1 . When the membrane form factor $F(q_z)$ is measured at several q_z values, a continuous function, $T(q_z)$, which is proportional to $F(q_z)$, can be fit to the data:^{10,32–34}

$$T(q_z) = \sum_n \sqrt{I_n} q_n \text{sinc}(\pi d_z q_z - \pi n). \quad (2)$$

Once an analytical expression for $T(q_z)$ has been determined from fitting the experimental peak intensities, the phases v_n can be determined from $T(q_z)$.

X-ray scans were measured for the pure DMPC bilayers and the DMPC–ethanol sample at two temperatures, namely $T = 293$ K, the gel phase for DMPC bilayers, and $T = 303$ K, their fluid phase. Data are shown in Fig. 4. A background scan of the glass substrate with Kapton polyimide foil was subtracted from the data shown in parts (a)–(d). The pronounced Bragg peaks at Q values up to $\sim 0.75 \text{ \AA}^{-1}$ were assigned to a multi-lamellar membrane structure in the powder. We find lamellar d_z spacings of $d_z^{\text{DMPC}} = 64.27 \text{ \AA}$, $d_z^{\text{DMPC-ethanol}} = 64.89 \text{ \AA}$ in the gel phase at $T = 293$ K and $d_z^{\text{DMPC}} = 61.10 \text{ \AA}$ and $d_z^{\text{DMPC-ethanol}} = 62.02 \text{ \AA}$ in fluid membranes. The measured d_z spacing for DMPC is in excellent agreement to lamellar spacings reported for fully hydrated bilayers.³⁵

The Bragg peaks were fit using Lorentzian peak profiles. Up to eight peaks could be fit and were used to reconstruct the electron density. $T(q_z)$ was fit to the experimentally determined peak intensities using eqn (2), where an array of v_n values was determined out of the corresponding 2^8 combinations, assuming a phase of $+1$ or -1 . The inset in Fig. 4(a) shows the best fit of $T(q)$ for DMPC in its gel phase as example. All samples were well fitted using the following combination of phases: $\bar{1}\bar{1}11\bar{1}\bar{1}11$. The resulting electron densities are plotted in Fig. 5.

We assign the additional correlation peak at higher Q values to the in-plane structure of the membranes. The lipid acyl chain positional correlation peak is the result of closely packed acyl chains making up the hydrophobic core of the membrane. The corresponding correlation peaks were observed at 1.49 \AA^{-1} in both the DMPC and DMPC–ethanol systems at $T = 293$ K, corresponding to a distance between neighbouring acyl chains of $\sim 4.21 \text{ \AA}$ in the gel phase. In the fluid phase, the lipid tail positional correlation peaks occur at 1.39 \AA^{-1} in the DMPC and DMPC–ethanol samples at $T = 303$ K, corresponding to an increased distance between neighbouring acyl chains of $\sim 4.53 \text{ \AA}$. The acyl chain correlation peak is more pronounced in the gel phase indicating a higher degree of order. The broad fluid peak is

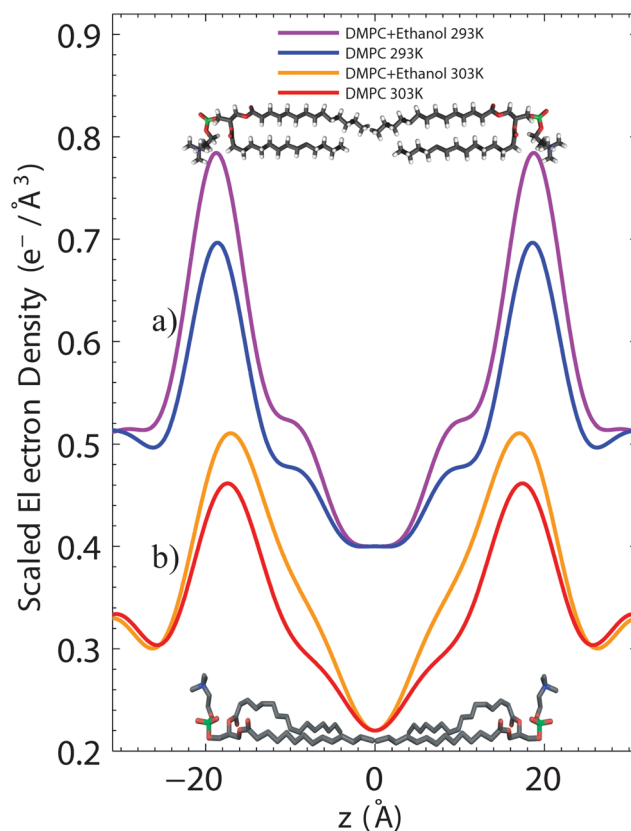


Fig. 5 Electron densities $\rho(z)$ for all sample variations, as determined from the data in Fig. 4, using eqn (1) and (2). $\rho(z)$ was scaled to the electron density of a CH_3 group in the centre (*i.e.* where lipid tail ends meet) and water or ethanol–water electron density at the ends (*i.e.* between the hydrophilic headgroups of adjacent bilayers). The 293 K data in (a) are shifted by $+0.18 \text{ e}^- \text{ \AA}^{-3}$ on the y -axis for clarity. $\rho(z)$ is increased in the presence of ethanol in the head-group region and at z -values around $\sim 9 \text{ \AA}$.

the fingerprint of the disordered L_α phase. The acyl chain packing is not significantly affected by the presence of ethanol as the position of the peak does not change with addition of ethanol within the resolution of this experiment. The weak peak at $\sim 1.1 \text{ \AA}^{-1}$ in Fig. 4 stems from the Kapton window and did not subtract perfectly; it is not related to a lipid membrane structure.

3 Results

3.1 Molecular freezing and melting studied by elastic neutron scattering

Elastic scattering data, during heating and cooling, are shown in Fig. 2. The heating curves have been shifted upward on the intensity axis to distinguish the transition locations. The original data shows closed loops for all plots indicating that the number of particles in the beam was constant during the experiments. Also, the system always returned to its initial high-temperature intensity.

Elastic scattering related to lipid diffusion is shown in Fig. 2(a) for pure DMPC and Fig. 2(b) for DMPC–ethanol. A pronounced step is observed at a temperature of $T = 297$ K. This temperature coincides well with the temperature of the main

transition in fully hydrated bilayers made of DMPC, which was reported at $T = 296.6$ K in multi-lamellar DMPC systems.^{19,22} The transition temperatures in Fig. 2(a) and (b) coincide, showing that within the temperature resolution of this experiment, ethanol does not change the temperature of the transition at this length scale. When comparing the pure DMPC and DMPC–ethanol, the introduction of ethanol does not change the elastic intensity in the fluid phase. In the gel phase, however, the elastic intensity changes drastically with the addition of ethanol. This is indicated by an increase in the slopes of the transitions at these lower temperatures and points to enhanced order in both gel and ripple phase due to ethanol.

An additional kink is observed at a temperature of $T = 286$ K, which can be assigned to the pre-transition in DMPC, *i.e.*, the transition between the gel (L_{β}) and ripple (P_{β}) phases of the bilayers. The pre-transition appears to be more pronounced in the presence of ethanol molecules and shifted by ~ 2.5 K towards higher temperatures (~ 288.5 K). No hysteresis was observed between the cooling and heating curve within the experimental resolution.

Nanoscale lipid tail dynamics are observed in Fig. 2(c) and (d). A pronounced step in the elastic intensity is observed at $T = 297$ K, related to the main transition. The transition temperatures in DMPC and DMPC–ethanol coincide; within the instrumental resolution, ethanol does not change the temperature of freezing or melting of the lipid acyl chains on nearest-neighbour distances of acyl chains. The step in the elastic scattering is, however, more pronounced in the presence of ethanol indicating a better ordered state in the P_{β} phase. No precise pre-transition temperature can be assigned to the data in Fig. 2(c) for pure DMPC on this length scale. However, a pronounced step associated with the transition into the L_{β} phase is observed in the presence of ethanol in Fig. 2(d) at ~ 288.5 K. In addition, the pre-transition temperature is slightly shifted towards higher temperatures. The transition appears more pronounced in the heating curve.

Dynamics of the hydration water are observed in Fig. 2(e) and (f). This detector is located at a Q position of $\sim 1.85 \text{ \AA}^{-1}$. This length scale is mainly sensitive to hydration water, which has a slightly lower density as compared to bulk water. A pronounced kink in the elastic intensity is observed at $T = 297$ K. The hydration water dynamics follow that of the lipid molecules and ethanol does not seem to change their dynamical behaviour. No hysteresis is observed; the ethanol does not seem to have an impact on the freezing and melting of the hydration water within the temperature resolution of this experiment.

3.2 Nanosecond membrane dynamics and diffusion studied quasi-elastic neutron scattering

QENS allows for the determination of lipid diffusion in the membranes. Exemplary QENS spectra of the DMPC–ethanol system at $T = 308$ K, in the fluid phase of the bilayers, are shown in Fig. 3 for two selected Q values. The instrumental resolution was determined from a Vanadium sample and it was found that rather than exhibiting a simple Gaussian peak shape, the resolution had a slight gradual asymmetry at negative $\hbar\omega$ values (fit with an asymmetric Gaussian) and a small shoulder at positive $\hbar\omega$ values (fit with an additional small Gaussian). The asymmetric Gaussian used to accommodate the gradual asymmetry in

the resolution function was composed of a Gaussian with an exponential function on one side of the peak,³⁶

$$y = y_0 + H(\hbar\omega_0 - \hbar\omega)Ae^{-\left(\frac{(\hbar\omega - \hbar\omega_0)^2}{2\sigma^2 + \tau|\hbar\omega - \hbar\omega_0|}\right)} + H(\hbar\omega - \hbar\omega_0)Ae^{-\left(\frac{(\hbar\omega - \hbar\omega_0)^2}{2\sigma^2}\right)}, \quad (3)$$

where A is the amplitude, ω_0 the elastic energy peak position, σ the Gaussian standard deviation, H is the Heaviside function, and τ the asymmetry parameter. For $\tau = 0$, a symmetric Gaussian function is obtained. Values of τ used to fit this gradual asymmetry ranged from ~ 0.030 to 0.217 . A Q range of $0.55 \text{ \AA}^{-1} < Q < 1.35 \text{ \AA}^{-1}$ was used for the determination of the diffusion constant.

The scattering obtained from the DMPC–ethanol sample is described by a narrow central component, corresponding to the instrumental resolution ($\sim 0.9 \mu\text{eV}$), a constant background, and a quasi-elastic broadening due to relaxational dynamics of the

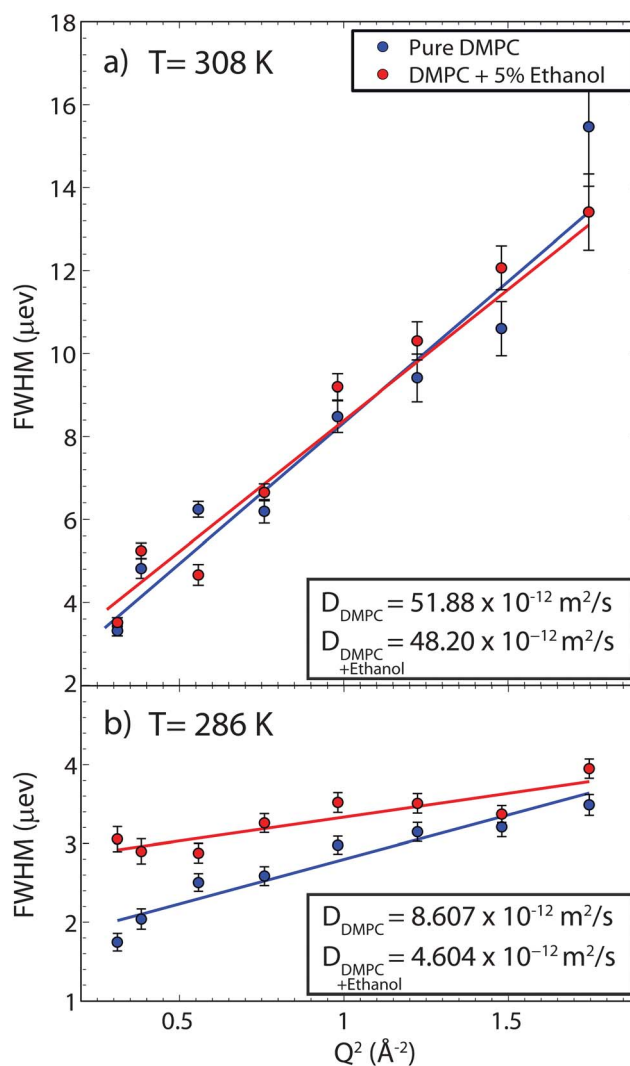


Fig. 6 FWHM of the quasi-elastic broadening as determined from the data in Fig. 3. Data are plotted as function of Q^2 such that the slope of the line is directly proportional to the diffusion coefficients.

lipid molecules. This broadening is fit with a Lorentzian function, convolved with the Gaussian instrumental resolution. It should be noted that the FWHM of the Lorentzian functions quoted in the paper are the deconvoluted values.

Fig. 6 displays the FWHM for all measured Q -values as a function of Q^2 . In this plot the FWHM scale linearly with Q^2 , a behaviour indicative of continuous diffusion ($\text{FWHM}_L = 2hDQ^2$), as previously explained in great detail in, *e.g.*, ref. 37. This behaviour was observed for the quasi-elastic broadening in the gel (P_{β}) and fluid phases of the DMPC and DMPC-ethanol bilayers, as shown in Fig. 6. The data fit is depicted by a blue line for the pure DMPC and red line for the DMPC-ethanol. From this linear fit the diffusion coefficients could be extracted and are displayed in Fig. 6. The values are in good agreement with diffusion coefficients quoted in the literature for similar systems.^{38–42} We note that the linear fit in Fig. 6 does not pass through the origin, as one would expect, and the offset is larger than the instrumental resolution. This effect is often observed in the literature, however no consistent explanation has been offered. We also note that the accessible Q range of the HFBS spectrometer is not sensitive to the ballistic diffusion regime³⁷ or a potential flow-like diffusion, as reported recently.⁴⁰

No difference in the diffusion constants in the fluid phase with or without ethanol was observed within the resolution of this experiment. The experimental values of the diffusion constants in the fluid phase are found to be $D_{\text{DMPC-ethanol}} = 48.20 \times 10^{-12} \text{ m}^2 \text{ s}^{-1}$ and $D_{\text{DMPC}} = 51.88 \times 10^{-12} \text{ m}^2 \text{ s}^{-1}$. Diffusion constants in the gel phase are significantly slower than in the fluid phase for both samples, with and without ethanol. However, diffusion in the gel phase in the presence of ethanol is slowed down by a factor of ~ 2 as compared to pure DMPC, as shown in Fig. 6(b). The diffusion constants in the gel phase are found to be $D_{\text{DMPC-ethanol}} = 4.604 \times 10^{-12} \text{ m}^2 \text{ s}^{-1}$ and $D_{\text{DMPC}} = 8.607 \times 10^{-12} \text{ m}^2 \text{ s}^{-1}$.

3.3 Electron densities and location of the ethanol molecules from X-ray scattering

The integrated intensities of out-of-plane Bragg peaks in Fig. 4 were used to calculate the electron density profile perpendicular to the bilayers following eqn (1). Position and partitioning of the ethanol molecules in the bilayers can then be determined from the different $\rho(z)$, shown in Fig. 5. In order to put $\rho(z)$ on an absolute scale, the electron densities were scaled to fulfil the condition $\rho(0) = 0.22 \text{ e}^- \text{ \AA}^{-3}$ (the electron density of a CH_3 group at the end of a lipid tail) in the centre of the bilayer, and the electron density of the solution outside the bilayers. The electron densities for water and water-5 wt% ethanol solution are calculated in Table 2. We find $\rho(d_z/2) = 0.330 \text{ e}^- \text{ \AA}^{-3}$ for water-5 wt% ethanol, and the well known $\rho(d_z/2) = 0.334 \text{ e}^- \text{ \AA}^{-3}$ for pure water.

The normalized electron density profiles for DMPC in its gel phase are depicted in Fig. 5(a). The profile corresponds to a DMPC molecule in the well ordered gel state with both chains in all-*trans* configuration, as has been reported previously.³¹ The electron rich phosphorous group in the head group region can be identified by the peak in the electron density at $\sim 22 \text{ \AA}$. $\rho(z)$ monotonically decreases towards the bilayer centre at $z = 0$; only CH_3 groups at the end of the lipid tails are found in the centre. The electron density profiles in the fluid phase in Fig. 5(b) agree well with profiles reported in the literature.^{31,43,44} The sharp dip at

Table 2 Properties of water, ethanol and the water-ethanol solution. The ethanol concentration is given as wt%, vol% and mol%. The calculated electron density is used to normalize the electron densities of the bilayers in Fig. 5 and 7

	Water (H ₂ O)	Ethanol (C ₂ H ₆ O)	Water-ethanol
% by weight (wt%)	—	—	5
% by volume (vol%)	—	—	6.25
% by moles (mol%)	—	—	2.02
Molecular weight (g mol ⁻¹)	18.0153	46.06844	18.58104
Molecules/Å ³	3.34×10^{-2}	1.03×10^{-2}	3.20×10^{-2}
Number of electrons	10	26	10.3
Electrons density (e ⁻ Å ⁻³)	0.334	0.268	0.330

the centre is the tell-tale sign of a fluid membrane, *i.e.*, the increasing number of kink-defects lower the density of the lipid tails in the bilayer centre.

The presence of ethanol leads to an increase in electron density in the head group region of the bilayers. $\rho(z)$ is also increased around z values of $\sim 9 \text{ \AA}$, representing the presence of molecules that have permeated the membrane. The dip in the electron densities at z values of $\sim 27 \text{ \AA}$ is most likely related to a reduced density of the hydration water and solvent at the lipid-solvent interface, as will be discussed below.

For a quantitative comparison, Fig. 7 shows the electron density profile of a single leaflet for each temperature in more detail. The increase in electron density is the result of the presence of additional molecules in the bilayers. The addition of two Gaussian peak profiles ($\rho(z) = \rho_0 \exp[-(z - z_0)^2/2\sigma^2]$) to the

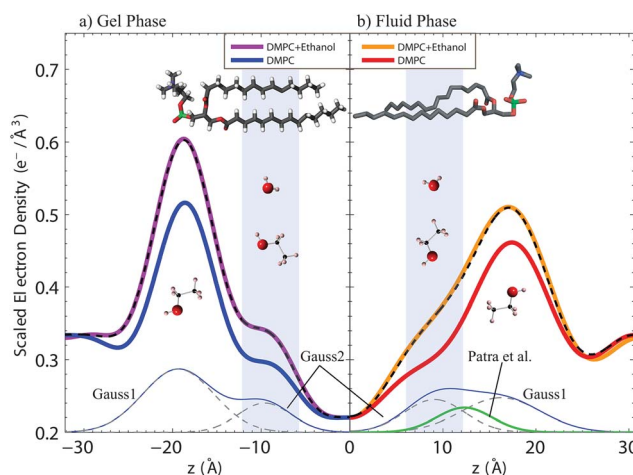


Fig. 7 Bilayer electron densities in gel and fluid phases. Each density is scaled to the electron density of CH_3 at the centre of the bilayer and the electron density of the respective solutes. One leaflet of a bilayer is shown. (a): In the gel phase, the electron density is increased in the presence of ethanol. The increase can be described by the addition of two Gaussian functions to the DMPC density (dashed black line). (b): In the fluid phase, an increase is seen in the presence of ethanol, which can also be described by two Gaussian distributions. The two Gaussians can be assigned to the presence of ethanol and possibly water molecules in the bilayers. The green Gaussian function is extrapolated from a mass density plot determined by a molecular dynamics simulation of DPPC and ethanol from Patra *et al.*⁷

Table 3 Parameters of the Gaussian peaks, $\rho(z) = \rho_0 \exp[-(z - z_0)^2/2\sigma^2]$, as determined from the fits in Fig. 7. Gaussian 1 is assigned to the presence of ethanol molecules in the head group region of the bilayers. Gaussian 2 can be assigned to additional ethanol (scenario ①) or water molecules (scenario ②) in the hydrophobic membrane core. Numbers are provided for both scenarios. Literature values have been used for the lipid areas in gel and fluid phase

	z_0 (Å)	ρ_0	σ (Å)	$\rho_0 \sigma \sqrt{2\pi}$ (Å ²)	d_z (Å)	A_L (Å ²)	#Electrons	#Molecules
Gauss 1 (gel)	19.35	0.087	4	0.872	64.89	47.2 (ref. 43)	0.654	1.58 ethanol–lipid
Gauss 2 (gel)	9.6	0.04	3	0.301	64.89	47.2 (ref. 43)	0.226	① 0.55 ethanol–lipid, ② 1.42 water–lipid
Gauss 1 (fluid)	16.25	0.0475	4.25	0.506	62.02	60.6 (ref. 31)	0.506	1.18 ethanol–lipid
Gauss 2 (fluid)	9.1	0.045	3.25	0.367	62.02	60.6 (ref. 31)	0.367	① 0.85 ethanol–lipid, ② 2.22 water–lipid

electron density profiles of pure DMPC in Fig. 7(a) and (b) results in the dashed black lines, which show excellent agreement to the DMPC–ethanol data. In the gel phase, Gauss 1 is centred at 19.35 Å and Gauss 2 is centred at 9.6 Å, whereas for the fluid phase we obtain the Gauss 1 centred at 16.25 Å and Gauss 2 centred at 9.1 Å. While Gauss 1 is dominant in the gel phase, Gauss 1 becomes comparable to Gauss 2 in the fluid phase in Fig. 7. Position, width and area of the Gaussian distributions in the different samples are summarized in Table 3.

The electron density of the lipid bilayer is defined by $\rho = e^-/V_L = e^-(A_L d_z)$, where V_L is the volume of a lipid molecule, A_L is the lipid area and d_z the lamellar spacing, *i.e.*, the size of the unit cell. One unit contains two lipid molecules and their hydration water molecules, as depicted in Fig. 5. The integral $e^- = A_L \int_0^{d/2} \rho(z) dz$ gives the total number of electrons in one leaflet. For pure DMPC this number is calculated to be $e_{\text{gel}}^- = 514$ and $e_{\text{fluid}}^- = 622$ in respective gel and fluid phases. Using the number of electrons per lipid (374, C₃₆H₇₂NO₈P) and water molecule (10, H₂O), these numbers refer to 1 lipid molecule hydrated by 14 water molecules in the gel phase, and 1 lipid molecule hydrated by 25 water molecules in the fluid phase, in excellent agreement to literature values.¹⁷ This agreement proves that our technique is capable to quantitatively determine electron densities, which is an important point for the discussion of partitioning of molecules below.

We note that the determination of lipid areas is an important field in membrane research. As discussed in detail in the literature,^{45,46} it is not straightforward to determine the area per lipid molecule directly from the inter-acyl chain correlation peak from the data in Fig. 4. Lipid areas can be determined with high accuracy by a combined approach using X-ray and neutron scattering and computer simulations, see ref. 29 for a recent review. We, therefore, used lipid areas published for DMPC in gel and fluid phases by the Nagle group^{31,43} (listed in Table 3). We also note that lipid areas can be determined from the chain correlation peaks in dehydrated gel phases, in the absence of lipid fluctuations.⁴⁷

The number of electrons related to the electron density in the Gaussian peaks can be calculated to $e^- = A_L \int_{\text{Gauss}} \rho(z) dz$. By dividing this number by the number of electrons of an ethanol or water molecule, the number of ethanol or equivalent water molecules per lipid molecule can be determined. As the X-ray experiment is averaging over a large number of those unit cells, a non-integer occupancy means that ethanol (or water) molecules can be shared between lipids. Partitioning of ethanol and water molecules in the lipid bilayers can be determined from these parameters and are calculated in Table 3.

4 Discussion

By combining X-ray diffraction and elastic and quasi-elastic neutron scattering, the molecular structure and dynamics of lipid membranes containing ethanol were determined. To the best of our knowledge this is the first extensive scattering study of the interaction of ethanol with lipid membranes. The bilayers were in contact with a 5 wt% water–ethanol solution, corresponding to 2 mol% of ethanol.

Electron density profiles in Figs. 5 and 7 allowed for the determination of the position of the ethanol molecules and their partition in lipid membranes. The presence of the ethanol molecules leads to an increase of the electron densities in both gel and fluid phases. The difference between $\rho(z)$ with and without ethanol is well described by the addition of two Gaussian distributions to the electron densities of pure DMPC bilayers. Gaussian 1 is centred at ~ 19 Å and ~ 16 Å in gel and fluid phases, in the head group region of the membrane. Gaussian 2 is centred at ~ 9 Å in gel and fluid phase, in the hydrophobic membrane core.

The positions of the two Gaussians can be compared to results from NMR^{1–3} and molecular dynamics simulations.^{7,8} Barry and Gawrisch located the ethanol molecules from NMR experiments close to the lipid–water interface for bilayers in the fluid phase in the region of the headgroup, glycerol backbone and the uppermost chain methylene groups. The position of ethanol molecules as determined from molecular dynamics (MD) simulations by Patra *et al.* (interpolated from Fig. 6 in ref. 7 and scaled by the ratio of the electron density to mass density of ethanol) is marked by the solid green distribution in Fig. 7(b). The MD simulations localize the ethanol molecules slightly closer to the membrane core, while NMR and X-ray diffraction experiments show good agreement finding the ethanol closer to the head group region in the membrane water interface. Therefore, we assign Gaussian 1 to ethanol molecules in the head group region of the bilayers in agreement with NMR studies.

The number of ethanol molecules in the head group region can be determined by further analysis of the areas of the Gaussian peaks. As listed in Table 3, the increase in electron density corresponds to ~ 1.6 ethanol molecules per lipid molecule in the gel phase at $T = 293$ K. Therefore, immersion of DMPC in a 2 mol% ethanol solution was found to result in a 1.6 molar concentration of ethanol in the head group region of the membranes. The number of ethanol molecules assigned to Gaussian 1 in the fluid phase is slightly less, ~ 1.2 ethanol molecules per lipid molecule.

Measuring membrane–ethanol and membrane–water partition coefficients in the presence of ethanol has proven to be difficult

due to experimental challenges, mainly related to the small volumes and the volatility of the ethanol molecule. Partition coefficients must be measured *in situ*, directly on lipid bilayers. Partitioning of ethanol in bilayers has been measured using different techniques:² radioisotopes,^{48,49} calorimetry^{9,50,51} and vapour pressure measurements.^{2,52} The molar coefficient of ethanol partitioning into lipid bilayers, K_p , is defined as $K_p = X_{\text{lipid}}^{\text{Et}}/X_{\text{water}}^{\text{Et}}$, where $X_{\text{lipid}}^{\text{Et}}$ and $X_{\text{water}}^{\text{Et}}$ are the mole fractions of ethanol in lipid and water phases, respectively. K_p can also be expressed using molar ratios $K_p = \frac{677.933}{18.015} \times \text{molar ratio}_{\text{lipid}}^{\text{Et}}/\text{molar ratio}_{\text{water}}^{\text{Et}}$, with $M_{\text{lipid}} = 677.933 \text{ g mol}^{-1}$ and $M_{\text{water}} = 18.015 \text{ g mol}^{-1}$ the molar masses of DMPC and water.

A K_p value of $K_p = 19$ was reported recently for POPC bilayers² at a water–ethanol concentration of 0.036 mol%. K_p s of $K_p \sim 8$, $K_p \sim 15$ (ref. 9) and $K_p \sim 28$ (ref. 51) were reported in DMPC. These coefficients correspond to molar concentrations on the order of ~ 1 mol%, *i.e.*, concentrations of 1 ethanol molecule per about 100 lipid molecules in the bilayers. We find 1.6 and 1.2 ethanol molecules per lipid molecule in gel and fluid phase, respectively. The fact that the coefficients reported in the literature^{9,49} have been determined in solutions with much smaller ethanol concentrations may point to a nonlinear partitioning of ethanol in lipid bilayers, in particular at higher alcohol concentrations. Our result is in agreement with computer simulations by Terama *et al.*,⁹ who observed almost complete partitioning of the ethanol molecules under similar conditions.

We now address the origin of the second Gaussian, inside the membrane core. The solubility of ethanol in the hydrophobic membrane core was found to be small in NMR experiments^{1,2} and computer simulations.⁶ However, Gaussian 2 partially overlaps with the z position of ethanol molecules reported from MD simulations,⁷ as shown in Fig. 7. In a more recent MD study using DPPC membranes in contact with a 1.9 mol% ethanol solution (see Fig. 4 in ref. 8) an additional peak was observed in the mass density of the bilayers near the bilayer centre, in agreement with the data in Fig. 7(b). The second Gaussian contribution might, therefore, be related to the presence of ethanol molecules in the hydrophobic membrane core. On the other hand, ethanol is also known to increase the permeability of lipid membranes for water molecules.^{53–56} Alternatively, the increase in electron density may, therefore, be due to an increase of the number of water molecules in the membrane in a 1.9 mol% water–ethanol solution.

Because we cannot unambiguously assign Gaussian 2 to the presence of either ethanol or water molecules, we would like to discuss two scenarios to explain the second Gaussian contribution centred at ~ 9 Å:

- (1) Gaussian 2 can be assigned to additional ethanol molecules in the hydrophobic membrane core.
- (2) Gaussian 2 can tentatively be attributed to water molecules in the bilayer, which have traveled into the hydrophobic core due to ethanol's effect of increased membrane permeability.

If Gaussian 2 is related to the presence of additional ethanol molecules in the membrane core, the increase in electron density corresponds to 0.55 ethanol molecules per lipid molecule in the gel phase and 0.85 ethanol molecules per lipid molecule in the fluid phase. It is believed that general anaesthetics, such as

ethanol, dissolve in membranes thereby changing their physical properties and altering membrane function.⁵⁷ Changes in lateral pressure is speculated to be relevant for protein function and binding sites, and in particular functioning of ion channels.⁵⁸ The potential presence of ethanol molecules in the hydrophobic core, as listed in Table 3, is likely to be important to distinguish between different theories.^{58–61} The presence and solubility of ethanol molecules in the hydrophobic core might also be relevant to model ethanol crossing event, as discussed in refs. 7–9.

When we assign Gaussian 2 to the presence of water molecules in the hydrophobic membrane core, the increase in electron density corresponds to 1.42 water molecules per lipid molecule in the gel state of the phospholipid membranes. In the fluid phase at $T = 303$ K (Fig. 7(b)), 2.22 water molecules per lipid molecule is dissolved in the hydrophobic membrane core.

The results from elastic and quasi-elastic neutron scattering give access to molecular membrane dynamics in the presence of alcohol. Lipid diffusion in the fluid phase is not altered by the presence of ethanol molecules in the bilayers, as shown in Fig. 6. The diffusion constant of $D \sim 50 \times 10^{-12} \text{ m}^2 \text{ s}^{-1}$ agrees well with diffusion constants reported in the literature for similar systems.^{38–42} This result is in excellent agreement to MD simulations, where no change in lateral diffusion coefficient was observed in the fluid phase of a DPPC membrane in contact with a 1.9 mol% ethanol solution.⁸ A similar behaviour was reported from MD simulations in DPPC, however, at very low ethanol concentrations.⁹ Diffusion is significantly slower in the gel phase when ethanol is present, consistent with the elastic data in Fig. 2. The inclusion of additional molecules to the head group region of the bilayers reduces the mobility of the lipid molecules in the more rigid gel phase, leading to a smaller diffusion constant.

Molecular freezing and melting is observed in the elastic neutron scattering experiments in Fig. 2. Molecular motions slower than about 1 nanosecond contribute to the elastic intensity. An increase in the recorded intensity is, therefore, caused by slowing down or freezing of molecular dynamics and can be used to assign phase transition temperatures and determine the “stiffness” of molecular interactions. The data in Fig. 2 show the effect of ethanol molecules on slow, nanosecond dynamics of the membranes on different length scales, corresponding to lipid diffusion, lipid tail and hydration water dynamics. Another important finding is that ethanol does not seem to change membrane properties in the fluid L_α phase as the elastic data coincide for DMPC and DMPC–ethanol for temperatures above 297 K. However, the absolute values of the elastic intensity are higher on all length scales in ripple and gel phase when ethanol is present, indicative of a better ordered lipid structure. This increased ordering in the ripple phase has been speculated to be a sign of interdigitation.¹²

The presence of ethanol molecules has a distinct effect on pre-transition (L_β to P_β) and main transition (P_β to L_α) of the membranes. All transitions appear more pronounced with ethanol. While the temperature of the main transition is not changed within the temperature resolution of 0.5 K of this experiment, the pre-transition was found to be shifted by ~ 2.5 K toward higher temperatures due to the presence of ethanol molecules.

These results lead us to the conclusion that ethanol has little effect on the nanosecond dynamics in the fluid phase of lipid

membranes. This type of dynamics includes diffusion, however also motions related to the elastic properties (e.g. undulation of the membranes), and molecular reorientations, which show relaxational dynamics. In a recent inelastic neutron scattering study ethanol was found to significantly increase the collective nanoscale dynamics of the lipid tails in the fluid phase of the membranes.¹¹ These dynamics are significantly faster than the dynamics probed here and happen on picosecond time scales and between neighbouring hydrocarbon tails. A new, low-energy phonon branch was observed in the presence of ethanol and speculated to be related to the mobility of kink defects perpendicular to the membranes, possibly responsible for the increased permeability for small molecules. While ethanol enhances molecular order in gel and ripple phases, likely ordering into a more densely packed structure, ethanol seems to mainly affect the fast collective dynamics in the physiologically relevant fluid phase.

Dynamics of the hydration water are observed in Fig. 2(e) and (f). A freezing and melting transition is observed as a kink in the elastic intensity curve at $T = 297$ K. This temperature coincides with the temperature of the main transition of the membranes. Hydration water dynamics, therefore, seem to be coupled to freezing and melting of membrane dynamics at the temperature of the main transition.

The freezing and melting transition of water, observed in detector D16, indicates that a significant fraction of the water molecules in our hydrated powder samples can be considered to be hydration water or membrane-bound water as opposed to bulk water. While a water–water correlation peak in bulk water would be observed at Q value $Q \sim 2 \text{ \AA}^{-1}$ (3.14 Å), we observe the nearest-neighbour distance between hydration water molecules to be increased by $\sim 8\%$ to 1.85 \AA^{-1} (3.4 Å) from the bulk water value. The dip in the electron densities in Fig. 5 and 7 at the lipid–solution interface at $z \sim 27 \text{ \AA}$, points to a reduced density of the hydration water density close to the lipid head groups. From the electron density plots, the dip is decreased by about 10% at the lipid–water interface, which agrees well with the decrease in density of the hydration solvent due to the increased nearest-neighbour distance.

5 Conclusion

In summary, we studied structure and dynamics of phospholipid membranes hydrated with a 5 wt% water–ethanol solution. Elastic and quasi-elastic neutron scattering was used to study slow, nanosecond molecular motions. By analyzing different length scales the effects of ethanol on diffusion, lipid acyl chain dynamics, and hydration water dynamics are determined. Lipid diffusion is found to be unaltered in the fluid phase ($D \sim 50 \times 10^{-12} \text{ m}^2 \text{ s}^{-1}$) however, decreased in the gel phase of the bilayers by 50%: from $D_{\text{DMPC}} = 8.607 \times 10^{-12} \text{ m}^2 \text{ s}^{-1}$ to $D_{\text{DMPC+ethanol}} = 4.604 \times 10^{-12} \text{ m}^2 \text{ s}^{-1}$. Ethanol is found to lead to a stiffer, better ordered structure in ripple and gel phases of the membranes. Another important finding is that the dynamics of membrane and hydration water are not significantly affected by the presence of ethanol in the physiologically relevant fluid phase of the membranes at this alcohol concentration.

However, our neutron experiments find the presence of ethanol molecules to have a distinct effect on the pre-transition

(L_{β} to $P_{\beta'}$) and main transition ($P_{\beta'}$ to L_{α}) of the membranes: all transitions appear more pronounced with the addition of ethanol. While the temperature of the main transition is not affected by ethanol, the pre-transition appears to be shifted to higher temperatures when ethanol is present.

From X-ray scattering experiments we determined the position of the ethanol molecules and their partitioning in the bilayers in gel and fluid phases. We find that the ethanol molecules are located in the head group region of the membranes, at a concentration of 1.6 ethanol molecules per lipid molecule in the gel phase, and 1.2 ethanol molecules per lipid molecule in the fluid phase. The electron densities give experimental evidence for an increased permeability in the presence of ethanol, related to either ethanol molecules in the hydrophobic membrane core or an enhanced permeability to water molecules. In future experiments neutron diffraction will be used to determine the number of ethanol and water molecules in the hydrophobic core by selectively deuterating ethanol molecules with respect to water in order to provide contrast between the two molecules. Partitioning of water and ethanol molecules is essential in better understanding the physiological effect of ethanol as a drug enhancer and an anaesthetic.

Acknowledgements

This research was funded by the Natural Sciences and Engineering Research Council of Canada (NSERC), the National Research Council Canada (NRC), the Canada Foundation for Innovation (CFI) and the Ontario Ministry of Economic Development and Innovation. We thank the NIST Center for Neutron Research for the allocation of beam time. This work utilized facilities supported in part by the National Science Foundation under Agreement No. DMR-0944772.

References

- 1 J. A. Barry and K. Gawrisch, *Biochemistry*, 1994, **33**, 8082–8088.
- 2 D. T. Nizza and K. Gawrisch, *Gen. Physiol. Biophys.*, 2009, **28**, 140–145.
- 3 L. L. Holte and K. Gawrisch, *Biochemistry*, 1997, **36**, 4669–4674.
- 4 S. E. Feller, C. A. Brown, D. T. Nizza and K. Gawrisch, *Biophys. J.*, 2002, **82**, 1396–1404.
- 5 J. Chanda and S. Bandyopadhyay, *Chem. Phys. Lett.*, 2004, **392**, 249.
- 6 A. N. Dickey and R. Faller, *J. Polym. Sci., Part B: Polym. Phys.*, 2005, **43**, 1025–1032.
- 7 M. Patra, E. Salonen, E. Terama, I. Vattulainen, R. Faller, B. W. Lee, J. Holopainen and M. Karttunen, *Biophys. J.*, 2006, **90**, 1121–1135.
- 8 A. N. Dickey and R. Faller, *Biophys. J.*, 2007, **92**, 2366–2376.
- 9 E. Terama, O. H. S. Ollila, E. Salonen, A. C. Rowat, C. Trandum, P. Westh, M. Patra, M. Karttunen and I. Vattulainen, *J. Phys. Chem. B*, 2008, **112**, 4131–4139.
- 10 T. Adachi, *Chem. Phys. Lipids*, 2000, **107**, 93–97.
- 11 M. D. Kaye, K. Schmalzl, V. C. Nibali, M. Tarek and M. C. Rheinstädter, *Phys. Rev. E: Stat., Nonlinear, Soft Matter Phys.*, 2011, **83**, 050907.
- 12 H. Seto, M. Hishida, H. Nobutou, N. L. Yamada, M. Nagao and T. Takeda, *J. Phys. Soc. Jpn.*, 2007, **76**, 054602.
- 13 P. Westerman, J. Pope, N. Phonphok, J. Doane and D. Dubro, *Biochim. Biophys. Acta, Biomembr.*, 1988, **939**, 64–78.
- 14 B. W. Koenig and K. Gawrisch, *J. Phys. Chem. B*, 2005, **109**, 7540–7547.
- 15 H. Komatsu and S. Okada, *Chem. Phys. Lipids*, 1997, **85**, 67–74.
- 16 H. V. Ly and M. L. Longo, *Biophys. J.*, 2004, **87**, 1013–1033.
- 17 E. Nováková, K. Giewekemeyer and T. Salditt, *Phys. Rev. E: Stat., Nonlinear, Soft Matter Phys.*, 2006, **74**, 051911.

- 18 M. C. Rheinstädter, T. Seydel and T. Salditt, *Phys. Rev. E: Stat., Nonlinear, Soft Matter Phys.*, 2007, **75**, 011907.
- 19 M. C. Rheinstädter, T. Seydel, F. Demmel and T. Salditt, *Phys. Rev. E: Stat., Nonlinear, Soft Matter Phys.*, 2005, **71**, 061908.
- 20 A. M. Gaspar, S. Busch, M.-S. Appavou, W. Haeussler, R. Georgii, Y. Su and W. Doster, *Biochim. Biophys. Acta*, 2010, **1804**, 7682.
- 21 A. Meyer, R. M. Dimeo, P. M. Gehring and D. A. Neumann, *Rev. Sci. Instrum.*, 2003, **74**, 2759–2777.
- 22 M. Weik, U. Lehnert and G. Zaccai, *Biophys. J.*, 2005, **89**, 3639–3646.
- 23 M. Doxastakis, V. García Sakai, S. Ohtake, J. Maranas and J. de Pablo, *Biophys. J.*, 2007, **92**, 147–161.
- 24 K. Wood, M. Plazanet, F. Gabel, B. Kessler, D. Oesterhelt, D. J. Tobias, G. Zaccai and M. Weik, *Proc. Natl. Acad. Sci. U. S. A.*, 2007, **104**, 18049–18054.
- 25 L. Toppozini, C. L. Armstrong, M. D. Kaye, M. Tyagi, T. Jenkins and M. Rheinstädter, *ISRN Biophysics*, 2012, **2012**, 520307.
- 26 M. C. Rheinstädter, J. Das, E. J. Flenner, B. Brüning, T. Seydel and I. Kosztin, *Phys. Rev. Lett.*, 2008, **101**, 248106, 4 pages.
- 27 V. García Sakai and A. Arbe, *Curr. Opin. Colloid Interface Sci.*, 2009, **14**, 381–390.
- 28 M. C. Rheinstädter, C. Ollinger, G. Fragneto, F. Demmel and T. Salditt, *Phys. Rev. Lett.*, 2004, **93**, 108107.
- 29 G. Pabst, N. Kučerka, M.-P. Nieh, M. Rheinstädter and J. Katsaras, *Chem. Phys. Lipids*, 2010, **163**, 460–479.
- 30 G. Fragneto and M. Rheinstädter, *C. R. Phys.*, 2007, **8**, 865–883.
- 31 S. Tristram-Nagle, Y. Liu, J. Legleiter and J. F. Nagle, *Biophys. J.*, 2002, **83**, 3324–3335.
- 32 J. F. Nagle and M. C. Wiener, *Biophys. J.*, 1989, **55**, 309–313.
- 33 J. Nagle, R. Zhang, S. Tristram-Nagle, W. Sun, H. Petrache and R. Suter, *Biophys. J.*, 1996, **70**, 1419–1431.
- 34 G. I. King and C. R. Worthington, *Phys. Lett. A*, 1971, **35**, 259–260.
- 35 N. Chu, N. Kučerka, Y. Liu, S. Tristram-Nagle and J. F. Nagle, *Phys. Rev. E: Stat., Nonlinear, Soft Matter Phys.*, 2005, **71**, 041904.
- 36 K. Lan and J. Jorgenson, *J. Chromatogr., A*, 2001, **915**, 1–13.
- 37 C. L. Armstrong, M. Trapp, J. Peters, T. Seydel and M. C. Rheinstädter, *Soft Matter*, 2011, **7**, 8358–8362.
- 38 C. L. Armstrong, M. D. Kaye, M. Zamponi, E. Mamontov, M. Tyagi, T. Jenkins and M. C. Rheinstädter, *Soft Matter*, 2010, **6**, 5864–5867.
- 39 W. Pfeiffer, T. Henkel, E. Sackmann and W. Knorr, *Europhys. Lett.*, 1989, **8**, 201–206.
- 40 S. Busch, C. Smuda, L. Pardo and T. Unruh, *J. Am. Chem. Soc.*, 2010, **132**, 3232–3233.
- 41 A. Buchsteiner, T. Hauß, S. Dante and N. Dencher, *Biochim. Biophys. Acta*, 2010, **1798**, 1969–1976.
- 42 S. König, W. Pfeiffer, T. Bayerl, D. Richter and E. Sackmann, *J. Phys. II*, 1992, **2**, 1589–1615.
- 43 N. Kučerka, Y. Liu, N. Chu, H. I. Petrache, S. Tristram-Nagle and J. F. Nagle, *Biophys. J.*, 2005, **88**, 2626–2637.
- 44 N. Kucerka, S. Tristram-Nagle and J. F. Nagle, *Biophysical Journal: Biophysical Letters*, 2006, **90**, L83–L85.
- 45 A. Spaar and T. Salditt, *Biophys. J.*, 2003, **85**, 1576–1584.
- 46 T. T. Mills, G. E. S. Toombes, S. Tristram-Nagle, D.-M. Smilgies, G. W. Feigenson and J. F. Nagle, *Biophys. J.*, 2008, **95**, 669–681.
- 47 M. A. Barrett, S. Zheng, G. Roshankar, R. J. Alsop, R. K. Belanger, C. Huynh, N. Kučerka and M. C. Rheinstädter, *PLoS One*, 2012, **7**, e34357.
- 48 Y. Katz and J. M. Diamond, *J. Membr. Biol.*, 1974, **17**, 69–86.
- 49 Y. Katz and J. M. Diamond, *J. Membr. Biol.*, 1974, **17**, 101–120.
- 50 E. S. Rowe, *Mol. Pharmacol.*, 1982, **22**, 133–139.
- 51 C. Trandum, P. Westh, K. Jørgensen and O. G. Mouritsen, *Biochim. Biophys. Acta*, 1999, **1420**, 179–188.
- 52 P. Westh and C. Trandum, *Biochim. Biophys. Acta*, 1999, **1421**, 261–272.
- 53 D. Huster, J. Jin, Albert, K. Arnold and K. Gawrisch, *Biophys. J.*, 1997, **73**, 855–864.
- 54 B. Deamer and J. Bramhall, *Chem. Phys. Lipids*, 1986, **40**, 167–188.
- 55 S. Paula, A. Volkov, A. Van Hoek, T. Haines and D. Deamer, *Biophys. J.*, 1996, **70**, 339–348.
- 56 G. Lahajnar, P. Macek, P. Smid and I. Zupancic, *Biochim. Biophys. Acta*, 1995, **1235**, 437–442.
- 57 P. Seeman, *Pharmacol. Rev.*, 1972, **24**, 583–655.
- 58 H. Jerabek, G. Pabst, M. Rappolt and T. Stockner, *J. Am. Chem. Soc.*, 2010, **132**, 7990–7997.
- 59 K. Pang, *Mol. Pharmacol.*, 1980, **18**, 84.
- 60 J. Trudell, *Anesthesiology*, 1977, **46**, 5.
- 61 D. Mountcastle, *Proc. Natl. Acad. Sci. U. S. A.*, 1978, **75**, 4906.